Supplementary information for: Insights into the Formation Mechanism of CdSe Nanoplatelets Using in situ X-ray Scattering

Nicolo Castro[†], Cécile Bouet[‡], Sandrine Ithurria[‡], Nicolas Lequeux[‡],
Doru Constantin[†], Pierre Levitz[¶], Diego Pontoni[§], Benjamin Abécassis[*,‖,†]
†Laboratoire de Physique des Solides,
CNRS, Univ. Paris-Sud, Université Paris-Saclay, 91405 Orsay Cedex, France
‡Laboratoire de Physique et d'Etude des Matériaux,
ESPCI-Paris, PSL Research University, Sorbonne Université, CNRS,
10 rue Vauquelin, 75005, Paris, France
¶Sorbonne Université, CNRS,
Physico-Chimie des Électrolytes et Nanosystèmes Interfaciaux, PHENIX, F-75005 Paris, France
§Partnership for Soft Condensed Matter (PSCM),
ESRF - The European Synchrotron,
71 Avenue des Martyrs, 38043 Grenoble, France

Contents

1 SAXS/WAXS experiments

The SAXS/WAXS experiments were performed on the ID02 beamline of the ESRF (European Synchrotron Radiation Facility) at an energy of 12.46 keV. The sample to SAXS detector distance was 1.5 m which yields a q-range of 0.067 to 4.5 nm^{-1}. A second detector was placed at 20 cm from the sample and allowed acquiring simultaneous WAXS data up to $q \simeq 32$ nm^{-1}. A Linkham hot stage was used to heat at a controlled rate the glass capillary and to acquire SAXS/WAXS patterns during the nanoparticle formation.

2 Synthesis of nanoplatelets

Two solutions were prepared: one containing the Cd precursor and one the Se precursor. The Se solution contains 85.4 mg of a stoichiometric TOP-Se solution obtained by mixing equal amount of trioctylphosphine and selenium mesh in equal molar amount and let under agitation in a glovebox overnight diluted in 2 mL of octadecene. The cadmium solution was obtained as follows: 80 mg of cadmium acetate di-hydrate, 700 μL of ethanol, 75 μL of oleic acid and 1.5 mL octadecene were mixed in a 20 mL scintillation vial. The solution was heated at 150 °C on a hot-plane for 2 hours to yield a cloudy white suspension. 40 μL of the Cd solution and 40 μL of the TOPSe solution were mixed together at ambient temperature just before the *in situ* experiment and the glass capillary was filled with this solution.

3 UV-VIS absorbance spectra and TEM of NPL obtained in capillary

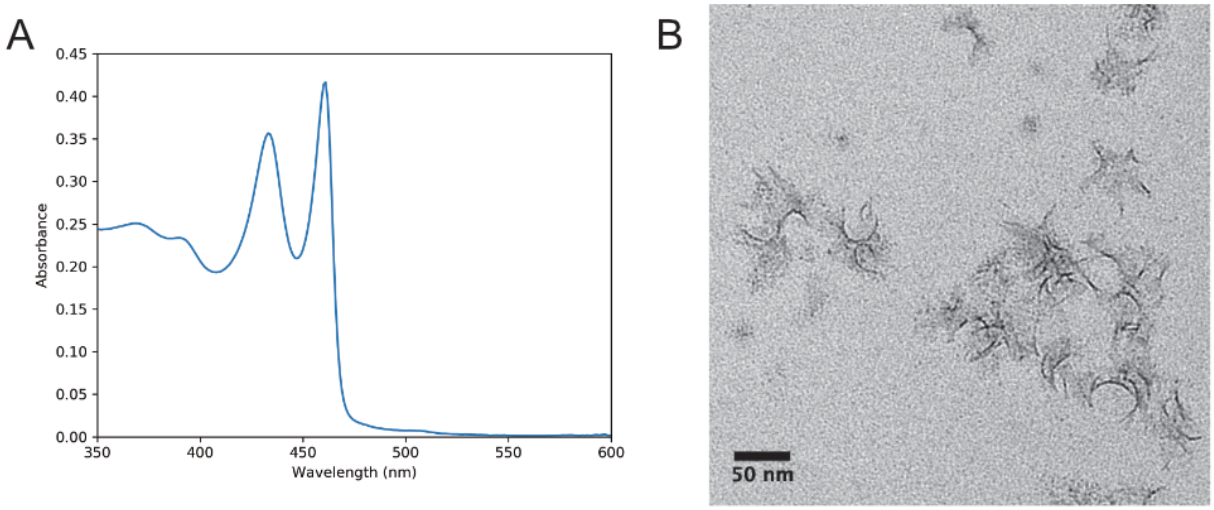

Figure S1: A) UV-VIS absorbance spectra, B) representative TEM image.

A typical UV VIS absorbance spectra and TEM images for NPL obtained in a capillary synthesis is shown on figure S1. These NPL have been obtained by heating at 200°C a solution containing an equal amount of the two following solutions: 1/ 50mg of Cd acetate and 60 μL of oleic acid dispered in 1 mL of ODE. 2/ 90 μL of saturated TOP-Se (2.24M) dispersed in 2 mL of ODE.

4 Fitting of the WAXS peak

Figure S2 shows the fitting of the (220) peaks with a pseudo-Voigt function. From the fitted parameters, the peak area, the lattice expansion with comparison to the bulk value and the typical length extracted from the full width at half maximum are shown in panels B,C and D.

5 SAXS modelling of curved nanoplatelets

The analytical expression for the signal obtained from curved platelets was taken from an article by Constantin [1] in which the form factor for a variety of bent platelets is derived. The orientationally-averaged form factor is calculated starting from the density distribution of the particle. Provided that no interaction exists between the scatterers, the scattering intensity can then be obtained from the form factor:

$$I(q) \propto |F(q)|^2 . \tag{1}$$

By using spherical/cylindrical coordinates and spherical harmonics, it is possible to simplify the integration and obtain the solution as a sum of functions. The system presented here is a platelet of size $L \times W \times t$, where L is the length, W is the width and t is the thickness of the platelet, bent around a circle of radius R, as shown in Fig.S3. For simplicity, during the mathematical derivation, the thickness of the particle will be considered negligible compared to the other dimensions, but is added in the simulations by multiplying by a correction factor [1]. Because of the shape of the particles, the obvious choice for the coordinate system is cylindrical coordinates, with the height of the platelet aligned along the z-axis. The density distribution of the particle can be separated in two different contributions: one, which we will call $G(r, \phi)$, the in plane contribution and the other, $H(z)$, along the main axis. The averaged form factor is then defined as:

$$|F(q)|^2 = \frac{1}{2}\int_0^{\pi} \sin(\theta) \left\langle \left|\tilde{G}(q_r, \eta)\right|^2 \right\rangle_{\eta} \left|\tilde{H}(q_z)\right|^2 d\theta, \tag{2}$$

where $\tilde{G}(q_r, \eta)$ and $\tilde{H}(q_z)$ are the Fourier transforms of $G(r, \phi)$ and $H(z)$ respectively, θ is the polar angle, $q_r = q \sin\theta$ and $q_z = q \cos\theta$. $\tilde{H}$ can easily be found by using a square function as a density distribution.

$$\tilde{H}(q_z) = \int_{-\infty}^{\infty} e^{-iq_z z} H(z) \begin{cases} H(z) = 1 & \text{if } -\frac{L}{2} \leq z \leq \frac{L}{2} \\ H(z) = 0 & \text{if } z < -\frac{L}{2} \text{ or } z > \frac{L}{2} \end{cases} . \tag{3}$$

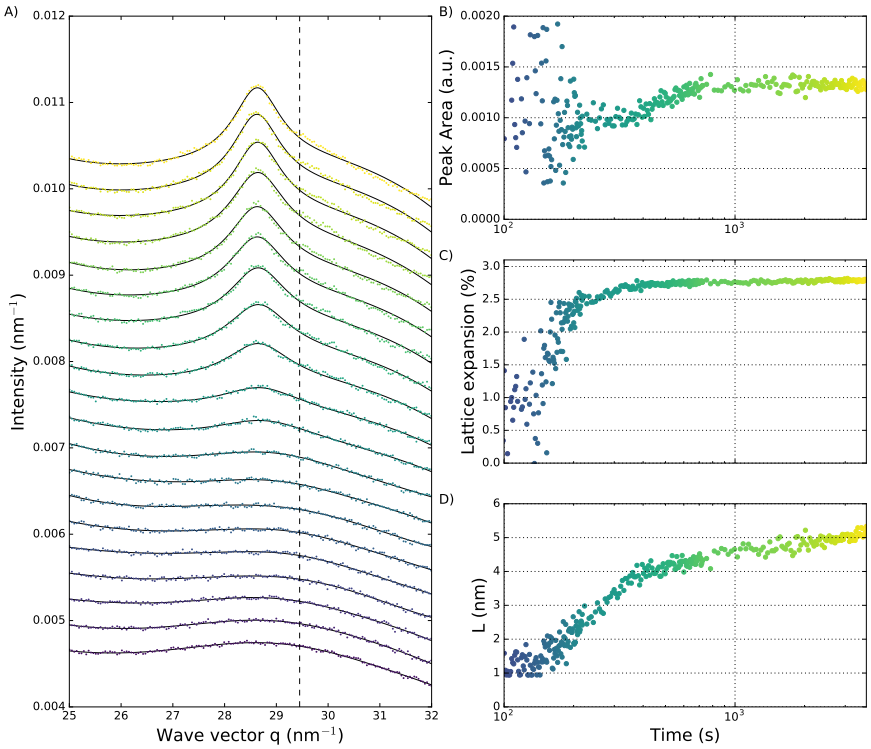

Figure S2: A) Fit of the (220) peak with a pseudo-Voigt function and a polynomial background. B), C) and D) relevant parameters extracted from the fit as a function of time.

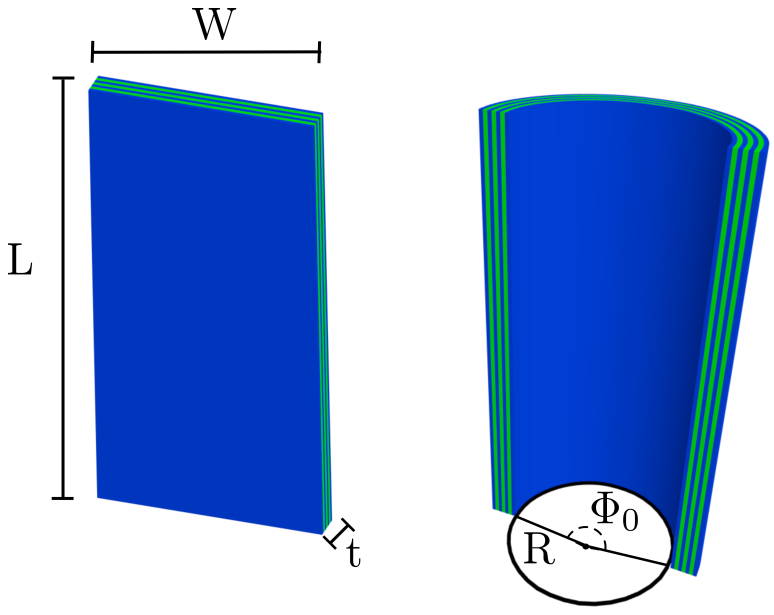

Figure S3: 3D rendering of a platelet showing the parameters used when referring to a curved platelet.

The derivation of the contribution from the *x*-*y* plane follows the same approach using polar coordinates and Bessel functions to obtain $\tilde{G}$ as an infinite sum:

$$\left\langle \left| \tilde{G}(q_r, \eta) \right|^2 \right\rangle = c^2 \left[J_0^2(q_r R) + 2 \sum_{k=1}^{\infty} a_k J_k^2(q_r R) \right]. \tag{4}$$

Here R is the curvature radius, J_k is the spherical Bessel function of order k and the coefficients $a_k = \left(\frac{\sin(k\phi_0/2)}{k\phi_0/2} \right)^2$, where $\phi_0 = W/R$ is the opening angle - the angle of the arc defined by the platelet. By doing the numerical calculation, it is possible to see that the contributions of the terms in the summation rapidly become negligible. No appreciable difference can be found by extending the calculations beyond the 15^{th} term. By using both of these definitions, the orientationally-averaged form factor simplifies from a triple integral (over η, z, and θ) to a single integral over θ.

In order to understand the effect of the different parameters on the SAXS patterns of curved NPLs, we computed series of intensity versus q curves for several sets of parameters: varying length, width and radiuses with the two other parameters being kept constant.

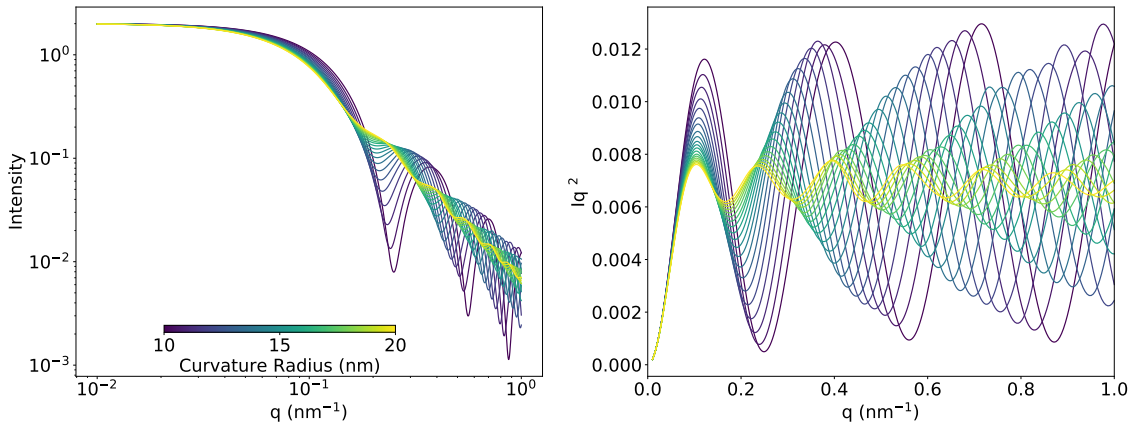

Figure S4: Simulated SAXS patterns for curved nanoplatelets with L=30, W=60 and a varying radius of curvature between 10 and 20 nm.

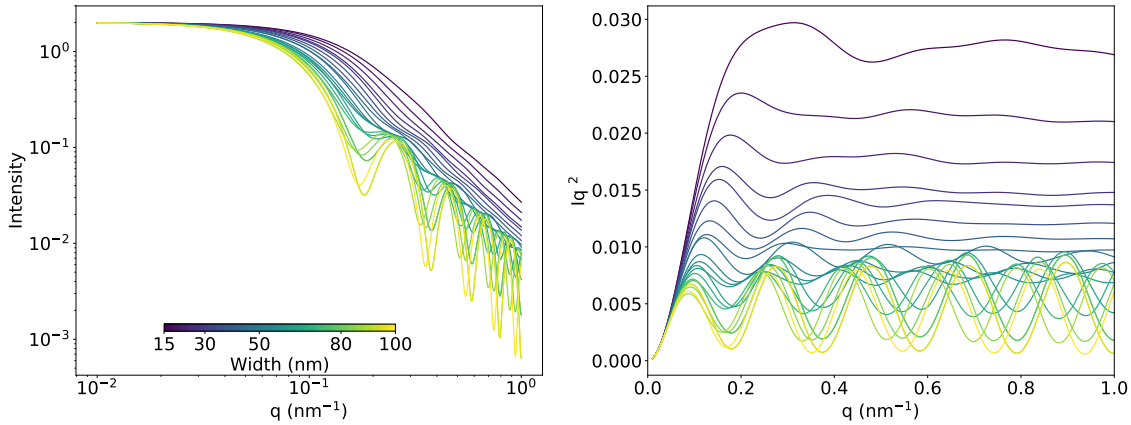

Figure S5: Simulated SAXS patterns for curved nanoplatelets with L =30 nm, R =15 nm and a varying width between 15 and 100 nm.

For $W = 60$, $L = 30$ nm and a radius of curvature increasing from 10 to 20 nm (figure S4) we see that the maximum of the first oscillation moves from 0.4 nm to 0.2 nm. The frequency of the oscillations also changes. Between q = 0.2 nm^{-1} and 1.0 nm^{-1} we count 5 oscillations for a radius of 20 nm and only 3 for 10 nm. We thus see that the position and the frequency of the oscillations is very sensitive to the radius of curvature. For R =15 nm and L = 30 nm the evolution of the SAXS pattern with varying width is shown on figure S5. For

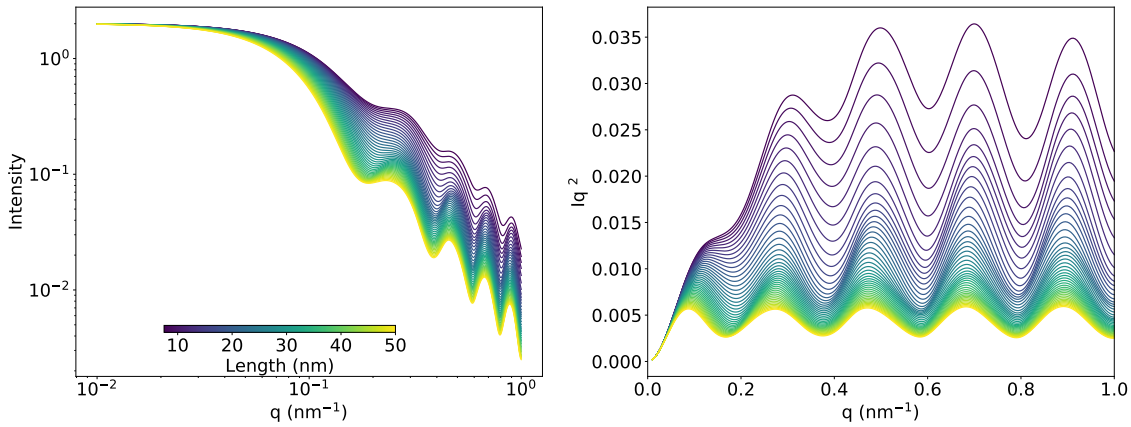

Figure S6: Simulated SAXS patterns for curved nanoplatelets with R =15 nm, W =60 nm and a varying length (L) between 7.5 and 50 nm.

small width, the curvature is hardly visible in the SAXS patterns and the Guinier regime is followed by a q^{-2} slope at higher q. This is understandable since the NPLs are not curved enough for its curvature to be visible at these length scales. When the width reaches 50 nm, oscillations start to appear whose position and frequency only weakly depend on the width. Finally, figure S6 shows the evolution of SAXS patterns for R =15 nm, W =60 nm and a varying L. The oscillations are visible for all the lengths tested and their position does not change as L varies. The larger the NPL, the earlier in q the decrease in intensity occurs as expected.

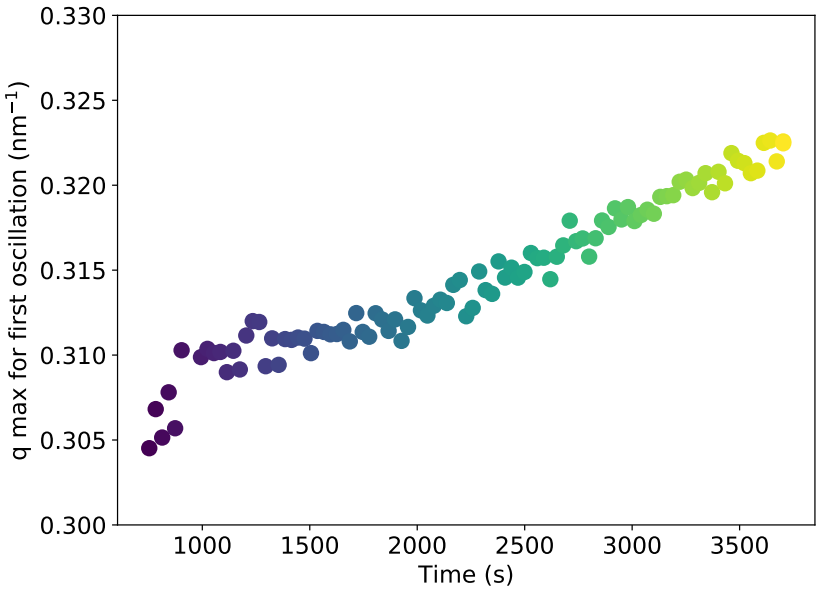

Figure S7: Position of the maximum of the first oscillations in the experimental SAXS patterns as a function of time.

6 Fit using a model of curved NPLs

The fit presented on figure 5 of the main text corresponds to the following intensity:

$$I(q) = I_{\text{NPLs}} + n \times I_{\text{mic}} + I_{\text{cap}} + b \tag{5}$$

where I_{NPLs} is the intensity of curved NPL as described in the previous section with a polydispersity on L and W. I_{mic} is a signal corresponding to small micelles. We evaluated this signal by fitting the SAXS pattern

before the onset of NPLs formation. It is best described by a polydisperse distribution of spheres with mean radius 0.3 nm and polydispersity of 80 %. Since the amount of micelles decrease with time as the precursors are consumed, we find $n < 1$. I_{cap} is the signal of the empty capillary. b is a constant background.

References

[1] Constantin, D. Solution scattering from colloidal curved plates: barrel tiles, scrolls and spherical patches. *Journal of Applied Crystallography* **48**, 1901–1906 (2015).